ACSNANO

www.acsnano.org

ARTICLE

Rapid Intestinal Uptake and Targeted Delivery to the Liver Endothelium Using Orally Administered Silver Sulfide Quantum Dots

Nicholas J. Hunt, Glen P. Lockwood, Frank H. Le Couteur, Peter A. G. McCourt, Nidhi Singla, Sun Woo Sophie Kang, Andrew Burgess, Zdenka Kuncic, David G. Le Couteur, and Victoria C. Cogger*

Cite This: *ACS Nano* 2020, 14, 1492–1507

Read Online

ACCESS | Metrics & More | Article Recommendations

ABSTRACT: Quantum dots (QDs) are used for imaging and transport of therapeutics. Here we demonstrate rapid absorption across the small intestine and targeted delivery of QDs with bound materials to the liver sinusoidal endothelial cells (LSECs) or hepatocytes *in vitro* and *in vivo* following oral administration. QDs were radiolabeled with ^{3}H-oleic acid, with a fluorescent tag or ^{14}C-metformin placed within a drug binding site. Three different biopolymer shell coatings were compared (formaldehyde-treated serum albumin (FSA), gelatin, heparin). Passage across the small intestine into mesenteric veins is mediated by clathrin endocytosis and micropinocytosis. 60% of an oral dose of QDs was rapidly distributed to the liver within 30 min, and this increased to 85% with FSA biopolymer coating. Uptake into LSECs also increased 3-fold with FSA coating, while uptake into hepatocytes was increased from 40% to 85% with gelatin biopolymer coating. Localization of QDs to LSECs was confirmed with immunofluorescence and transmission electron microscopy. 85% of QDs were cleared within 24 h of administration. The bioavailability of ^{14}C-metformin 2 h post-ingestion was increased 5-fold by conjugation with QD-FSA, while uptake of metformin into LSECs was improved 50-fold by using these QDs. Endocytosis of QDs by SK-Hep1 cells (an LSEC immortal cell line) was *via* clathrin- and caveolae-mediated pathways with QDs taken up into lysosomes. In conclusion, we have shown high specificity targeting of the LSEC or hepatocytes after oral administration of QDs coated with a biopolymer layer of FSA or gelatin, which improved the bioavailability and delivery of metformin to LSECs.

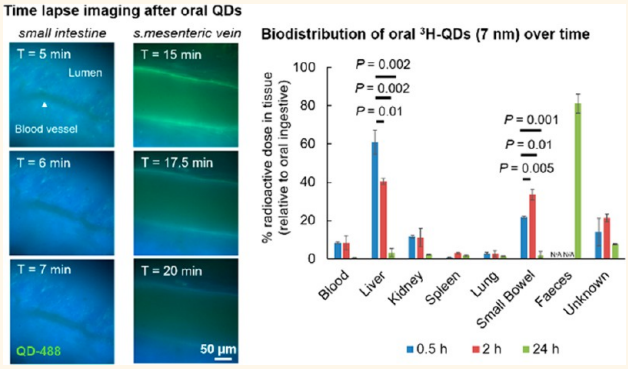

KEYWORDS: *mice, metformin, endocytosis, biopolymer, nano*

The initial use of quantum dots (QDs) in a biological setting was reported by Chan *et al.*[1] and Bruchez *et al.*,[2] who produced water-soluble CdSe/ZnS (core/shell) QDs with transferrin polymer capping. These QDs were endocytosed by HeLa cells and 3T3 mice fibroblasts as shown by fluorescence microscopy. Since that time, there has been increasing interest in the potential use of QDs for imaging and targeted delivery of pharmacotherapeutic agents.

Parenterally administered nanomaterials are extensively taken up by the liver, spleen, and kidneys.[3] Within the liver, uptake of nanomaterials is primarily mediated by Küpffer cells (KCs) and to a lesser extent by B lymphocytes and liver sinusoidal endothelial cells (LSECs).[3] Uptake of nanomaterials by KCs and LSECs reflects their capacity for avid phagocytosis and endocytosis of circulating particles, respectively.[4]

One of the goals driving the development of nanomedicines is to provide targeted drug delivery to specific cell types, particularly certain cancer cells. Structural modifications, such as poly(ethylene glycol) coatings, modify their biodistribution to either reduce the clearance of nanomaterials by the liver[5] or to improve delivery to cell types such as KCs,[6] LSECs,[7] tumor LSECs,[8] or KCs/hepatocytes.[9] Yu *et al.*[7] showed that α-melittin coated lipid/cholesterol-based nanoparticles (NPs) had a 2.7-fold greater affinity for LSECs than KCs, compared

Received: August 1, 2019
Accepted: January 22, 2020
Published: January 24, 2020

https://dx.doi.org/10.1021/acsnano.9b06071
ACS Nano 2020, 14, 1492–1507

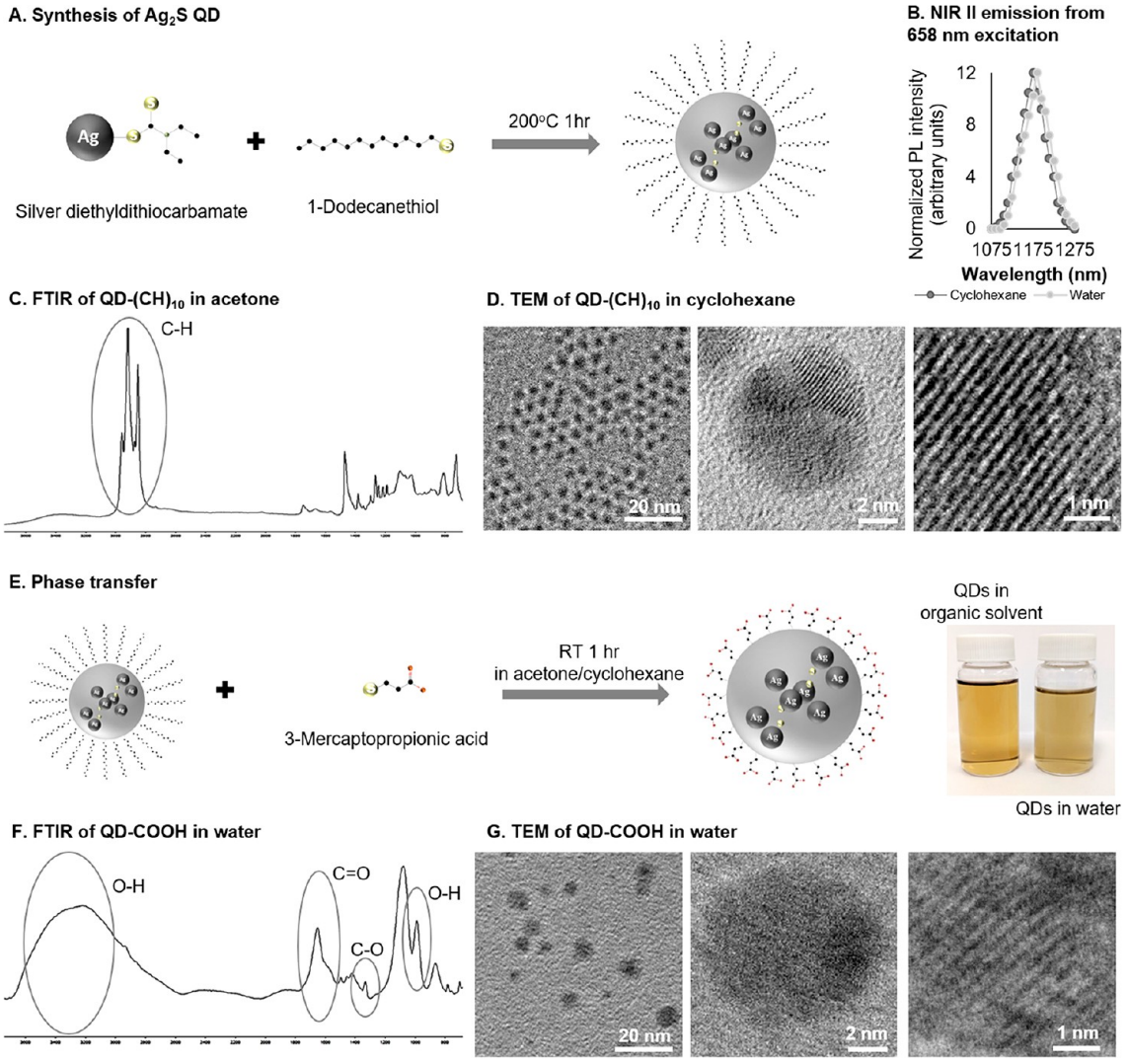

Figure 1. Synthesis and characterization of water-soluble Ag_2S QDs. (A) Schematic illustrating production of cyclohexane soluble QDs. (B) NIR II emission of QDs in cyclohexane at 1175 nm and in water at 1185 nm from 658 nm excitation. (C) FTIR spectra demonstrating dodecane C−H chains on the surface of QDs. (D) TEM images of QDs showing arrangement, size, and lattice structure. (E) Schematic of phase transfer of carboxylic acid (COOH) capped QDs with representative samples of 1 mM QDs in organic solvent and water. (F) FTIR spectra showing OH functional group with C═O, C−O, and OH fingerprints. (G) TEM images of monodispersed QDs in water.

to noncoated lipid/cholesterol NPs that had a 50:50 biodistribution. The study also showed that their NPs accumulated within the liver and the adrenal gland/kidney. To date, the oral administration of such nanomedicines has remained a challenging problem.

It has been reported that CdSe/CdS QDs are taken up by LSECs, KCs, and isolated human umbilical vein endothelial cells, but not by hepatocytes[10] and that these QDs accumulate in the kidneys and are still present 30 days later.[11] This accumulation in combination with evidence that CdSe QDs contribute to renal toxicity has led to a shift toward Cd-free QDs.[12] Another concern for biological applications of QDs is the generation of reactive oxygen species.[12] Ag_2S QDs have been shown to be nontoxic in terms of reactive oxygen species generation, cell proliferation, apoptosis/necrosis, and DNA damage in mouse fibroblast L929 cell lines when compared to CdSe/ZnS QDs.[13] The uses of Ag NPs are not restricted to the biomedical field with these particles also being utilized in the food industry as health supplements and within processing and food packaging.[14]

The potential role of Ag-based nanomedicines for targeting LSECs has not been reported. Pathological changes in the LSECs are a feature of several liver diseases including hepatic fibrosis and cirrhosis as well as aging.[15,16] We have shown that several agents can influence LSECs ultrastructure (including metformin, sildenafil, amlodipine, bosentan, and 2,5-dimethoxy-4-iodoamphetamine) with potential impact on transfer of substrates between the blood and hepatocytes, and hence liver function more generally.[17,18] The targeted delivery of these agents to LSECs by nontoxic NPs such as Ag_2S QDs could therefore represent a therapeutic approach for the treatment of some liver diseases and age-related changes in the liver.[16] Here we aimed to develop Ag_2S QDs that target the LSEC and hepatocytes after oral administration and to characterize their biodistribution and uptake.

RESULTS AND DISCUSSION

Synthesis and Characterization of the Ag_2S QD Platform with Various Biopolymer Coatings. We previously generated CdTe/CdS QDs with a particle diameter

https://dx.doi.org/10.1021/acsnano.9b06071
ACS Nano 2020, 14, 1492−1507

Table 1. Characterization of Ag_2S Quantum Dots with Different Biopolymer Coatings

characterization	Ag_2S QD COOH	Ag_2S QD FSA	Ag_2S QD heparin	Ag_2S QD gelatin
size (nm), shape (spherical)	7.3 ± 1.3	7.8 ± 1.1	6.8 ± 0.9	8.9 ± 1.4
hydrodynamic diameter (nm)	30 0.0 ± 2.0	72.5 ± 5.3	63.4 ± 4.9	89.9 ± 8.8
ζ potential	−29.3 ± 0.6	−35.2 ± 0.7	−31.3 ± 0.9	−27.2 ± 1.4
labels used	^{3}H OA, 488-TPR	^{3}H OA, 488-TPR	^{3}H OA, 488-TPR	^{3}H OA, 488-TPR
^{3}H OA label concentration	0.05 μCi (110,000 DPM)	0.05 μCi (110,000 DPM)	0.05 μCi (110,000 DPM)	0.05 μCi (110,000 DPM)
488 label concentration (QD:488 TPR; mol/mol)	1 mM:1 mM	1 mM:1 mM	1 mM:1 mM	1 mM:1 mM
biopolymer	none	formaldehyde-BSA	unfractionated heparin	gelatin
biopolymer concentration (QD: polymer; μg/mL)	N/A	250:500	250:500	250:500

of 2.1 nm and a hydrodynamic diameter of 3.7 nm. These QDs were selectively taken up by LSECs a few minutes after intravenous injection.[10] However, cadmium QDs are toxic, and oral bioavailability is uncertain which limits the usefulness of these QDs in animals or humans.[12] Therefore, we synthesized Ag-based QDs because these are less toxic, and on the basis of the CdTe/CdS QD experiments, we hypothesized that these would also be taken up selectively by LSEC if they had a similar diameter. We also proposed that selective uptake by LSECs would be enhanced if the QDs were coated with protein biopolymers that are avidly endocytosed by LSECs.

The colloidal solution-phase synthesis of carbon chain capped Ag_2S QDs and phase transfer to carboxylic acid capping are shown in Figure 1. The Ag_2S QDs were characterized for size, shape, hydrodynamic diameter, ζ potential, radioactive and florescence labeling, and biopolymer concentrations (Table 1). QDs with and without biopolymer coating were monodispersed in water or PBS and demonstrated a preserved lattice spacing of 0.25 nm (Figure 1). The QDs had a diameter of 7.3 ± 1.3 nm with a hydrodynamic diameter of 30.0 ± 2.0 nm, which increased substantially following biopolymer attachment. The ζ potential for the coated and uncoated QDs was approximately −30 mV, indicating moderate stability of the QD colloidal suspension (Table 1).

The protein corona is a mixture of biological proteins and/or other materials that coat nanomaterials following ingestion or injection into a biological model.[19] Examination of the protein corona of Ag_2S QDs was performed by incubating QDs for 24 h with RPMI media, 1 mg/mL bovine serum albumin (BSA), or mouse serum plasma. Fourier transformed infrared microscopy (FTIR) analysis demonstrated protein bound to the surface of QDs (Figure 2A−D) with the emergence of amine functional groups on the surface of the inorganic QDs. Both BSA and serum incubation highlighted similar patterns of amine I and II fingerprint spectra, indicating that serum incubation promotes albumin coupling to Ag_2S QDs in plasma (Figure 2A−D).

We then coated the QDs with one of three different protein biopolymers in order to increase selective uptake by LSECs. LSECs are responsible for highly efficient clearance of blood-borne macromolecules *via* endocytosis mediated by various membrane receptors.[4] In particular, LSECs avidly endocytose formaldehyde-treated serum albumin (FSA), collagen degradation product,s and heparin.[4] Therefore, we generated QDs coated with either FSA, heparin, or gelatin. FSA, heparin, or gelatin biopolymers demonstrated differential and distinct QD surface topology as determined by FTIR (Figure 3A−C). FTIR analysis showed biopolymer coating promoted amine

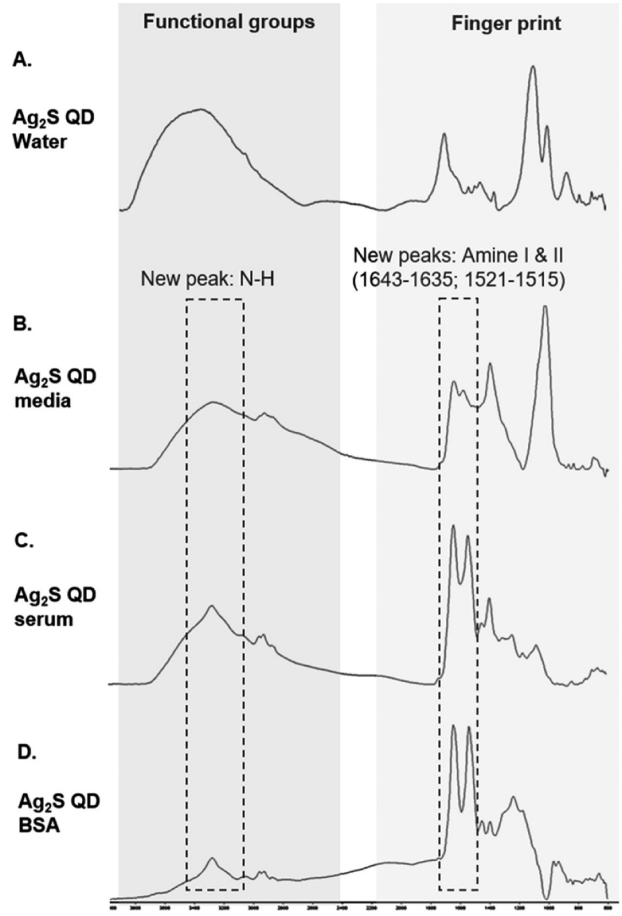

Figure 2. Protein corona surface topology alterations to QDs. (A) FTIR of water-soluble QD. (B−D) Formation of the protein corona following 24 h incubation with (B) RPMI media, (C) mouse serum, and (D) BSA. Protein corona demonstrates formation of amine functional groups (amines I and II). Gray insert boxes show raw material FTIR spectra with gray arrows showing OPUS wizard identified determinant peaks. Binding of biopolymer to QDs was performed using click chemistry (EDC/NHS coupling).

functional group expression with each coating promoting different expression patterns of amines I, II, and III within the fingerprint region of the spectra (Figure 3A−C). FTIR spectra of QD-FSA, QD-heparin, and QD-gelatin demonstrated similar spectra to the biopolymer alone (Figure 3A−C).

The stability of the fluorescent biopolymer attachment to the QDs was examined by incubation at pH 3, 5, 7, 9, and 11 for 4 h. Following incubation, QDs were centrifuged and

https://dx.doi.org/10.1021/acsnano.9b06071
ACS Nano 2020, 14, 1492−1507

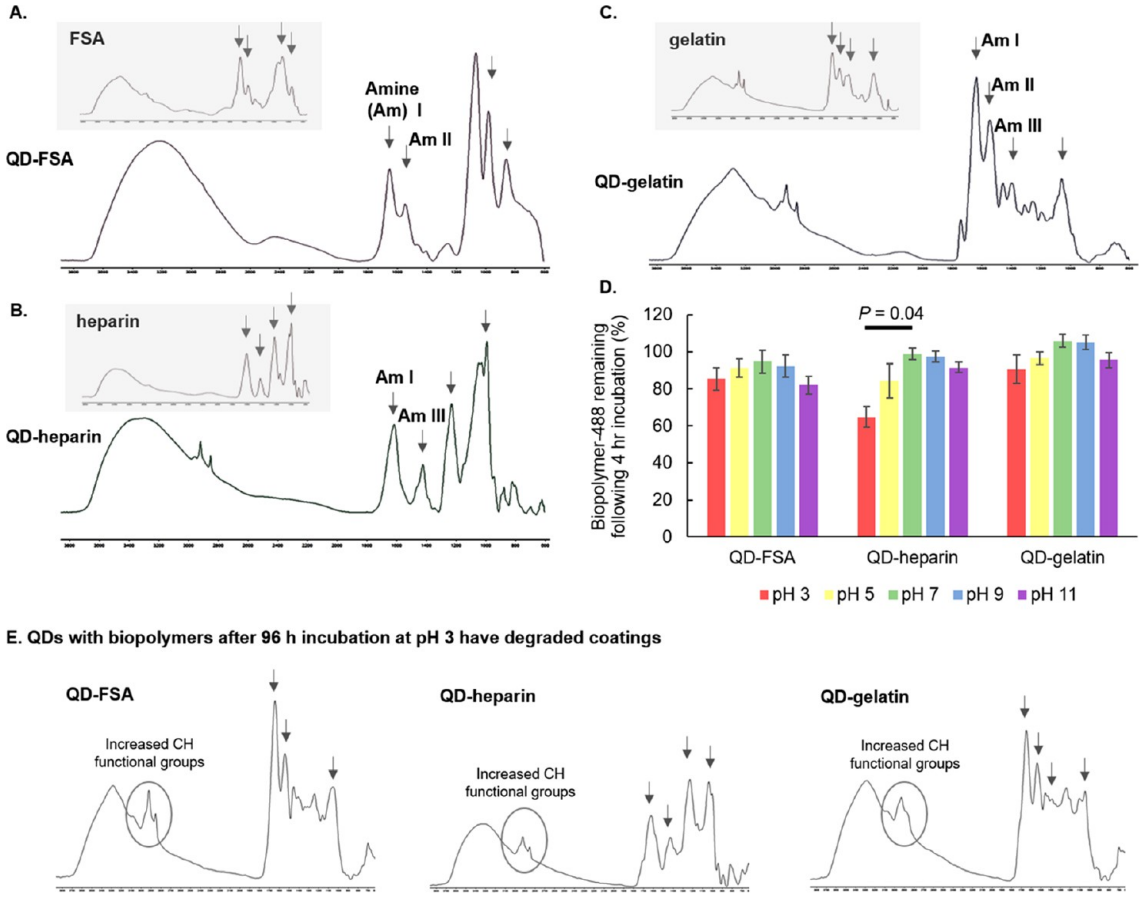

Figure 3. Biopolymer surface coatings on QDs. Gray insert boxes show raw material FTIR spectra with gray arrows showing OPUS wizard identified determinant peaks. Binding of biopolymer to QDs was performed using click chemistry (EDC/NHS coupling). QD-FSA (A), QD-heparin (B), and QD-gelatin (C) all demonstrated similar FTIR spectra to the raw biopolymer. Black arrows show OPUS wizard identified determinant peaks, which corresponded to peaks shown in the insets. Peaks identified were amines I, II, and III. (D, E) Following of biopolymer with 488 to QDs, samples were incubated at different pHs for 4 h, centrifuged and washed, and examined for 488 fluorescence. (E) Samples were incubated for 96 h at pH 3, centrifuged and washed, and examined using FTIR. Similar peak expression was observed with increased carbon chain functional groups.

resuspended, and the remaining fluorescence attached to the QDs was quantified. No change in QD-FSA or QD-gelatin 488 fluorescence was observed at pH 3, 5, 9, or 11 compared to QDs incubated at pH 7 (Figure 3D). QD-heparin exhibited a 30% reduction in fluorescence following pH 3 incubation (Figure 3D). The use of a linker protein during conjugation may contribute to weaker stability. Prolonged incubation (96 h at pH 3) of QD-biopolymers led to increased CH functional groups and loss of distinct fingerprint spectra, however no loss of biopolymer attachment from QDs was observed (Figure 3E). Four h of incubation did not lead to changes in FTIR spectra.

Biodistribution of Gavaged Ag_2S QDs. Oral administration of nanocarriers such as QDs is a key challenge for nanomedicine development, and various strategies have been explored to their improve oral bioavailability.[20] Kim *et al.*[21] obtained a 47% oral bioavailability using bile-acid-conjugated polystyrene NPs with 100 nm diameter and 18% for those with 250 nm diameter, *via* uptake into the intestinal lymphatics.

Wang *et al.*[22] modified mesoporous silica NPs with cationic cell-penetrating peptides under a hydrophilic succinylated casein layer, which increased the oral systemic bioavailability of its cargo, paclitaxel, nearly 8-fold.[22] Kang *et al.*[23] used gold-based NPs coated with glycol chitosan and taurocholic acid to successfully deliver siRNA to liver metastases after oral dosing. However, to date most studies of QDs have used parenteral modes of administration. We were interested in the oral administration of QDs because our target cells are LSECs, which are the first organ-based cells exposed to orally administered drugs once they have been absorbed and traversed the portal vein. Moreover, orally administered drugs can act on LSECs (and the liver) without the need for any systemic bioavailability and exposure, thus reducing the risk of systemic adverse effects. However, there have been few, if any, reports that QDs have substantial oral bioavailability.

Our ^3H radiolabeled Ag_2S QDs demonstrated rapid (under 30 min) accumulation in the liver following ingestion. To further investigate this observation of rapid transfer across the small intestine, Ag_2S QDs conjugated to Alexa Fluor 488 were gavaged, and time lapse imaging in live mice was performed of the small intestine (Figure 4A). Live imaging demonstrated that the QD-488 signal accumulates between the villi of the intestine. The blood vessels of the intestine demonstrate a 488 fluorescent signal 5 min following gavage of QD-488. Time lapse imaging shows the progression of 488 signal from the lumen to the blood vessel (Figure 4A). Imaging of the superior mesenteric vein following gavage demonstrated 488 fluorescence that gradually reduced over time (Figure 4B). ^3H-QDs

https://dx.doi.org/10.1021/acsnano.9b06071
ACS Nano 2020, 14, 1492−1507

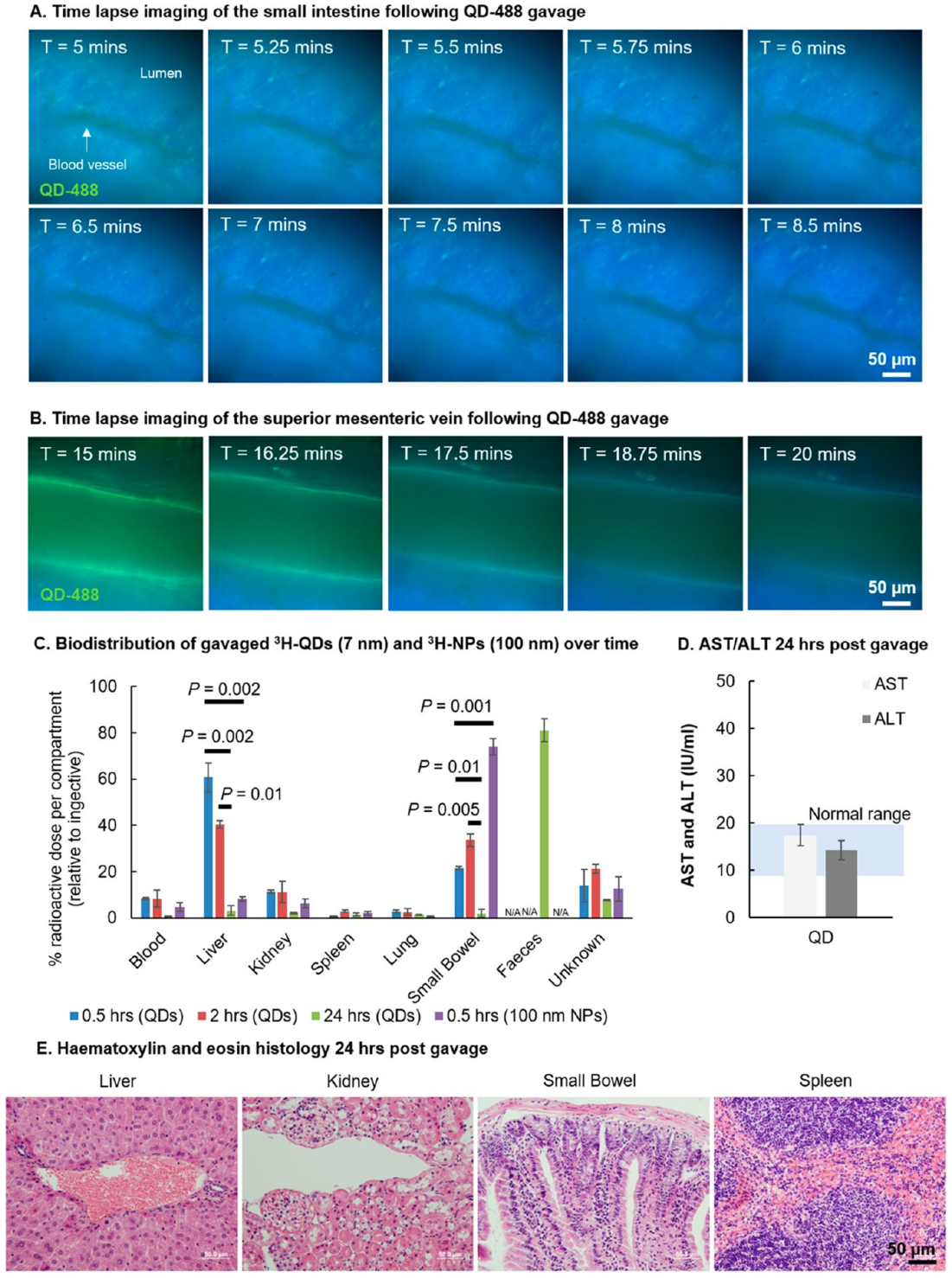

Figure 4. The lifecycle of Ag_2S QDs following gavage. (A) Time lapse images of QD-488 following gavage and anesthetize in mice. Following anesthesia, the small intestine was isolated and imaged. All times shown are from the time of gavage. 488 florescence was observed in the blood vessels lining the small intestine and appeared to transverse toward the blood vessels over time (5−8.5 min). (B) At 15−20 min, imaging was performed of the superior mesenteric vein; this vessel demonstrated 488 fluorescence that progressively reduced over time. (C) Biodistribution of ^{3}H-QDs was measured at 30 min, 2 h, and 24 h post-gavage of 100 μL of 1 mM QDs. ^{3}H-Ag_2S NPs (100 nm diameter) localization was also examined. Thirty min post-gavage, the liver demonstrated 60% accumulation of the ingested radioactive QDs with minimal expression in other organs. Two hr post-gavage, the liver demonstrated 40% expression of the ingested radioactive QDs with the small bowel showing increased radiation. At 24 h post-gavage, fecal matter demonstrated 85% of the ingested radioactive dosage with minimal expression observed in the organs. NPs were observed mostly in the small bowel only. (D) Liver function tests were performed using AST and ALT assays using blood samples collected 24 h post-gavage with QDs. (E) H&E stained tissue samples from the liver, kidney, small bowel, and spleen demonstrated no immune cell infiltration or cellular necrosis.

https://dx.doi.org/10.1021/acsnano.9b06071
ACS Nano 2020, 14, 1492−1507

accumulated in the liver (60% of the ingested dosage) 30 min after gavage of 100 μL of 1 mM (250 μg/mL) QDs (Figure 4C). Experiments with tissue collected at 2 h post-dose demonstrated a reduction in liver radioactive content and a marginal increase in small intestine radiation compared to samples collected at 30 min post-gavage (Figure 4C). During the 24 h after gavage, accumulated fecal matter was observed to contain 85% of the ingested radioactivity, and very low radiation was observed in the liver and small intestine tissues collected 24 h after gavage, consistent with biliary excretion (Figure 4C). Blood collected from the portal vein contained 5−10% of the dose, raising the possibility of enterohepatic recirculation. Comparing radiolabeled Ag_2S QDs with Ag_2S NPs (100 nm diameter), it was observed that 30 min following gavage NPs do not clear the small intestine (Figure 4C). This suggests that 100 nm NPs do not enter the enterohepatic circulation, while 7−8 nm QDs enter this circulation but not the systemic circulation. Entry into the systemic circulation is thus dependent on smaller nanomaterial sizes, coatings, and material properties.

Initial toxicity studies were undertaken. Aspartate transaminase (AST) and alanine transaminase (ALT) levels were not different to untreated controls (Figure 4D). H&E analysis of liver tissue did not show any immune cell infiltration or cellular necrosis following QD administration (Figure 4E).

To investigate the uptake pathways of our radiolabeled QDs in the small intestine, we examined the endocytosis pathways involved using intestinal explants. Explants of the small intestine tissue have previously been applied by Danielsen *et al.*[24] Measurement of QD uptake was performed based on ^3H radiolabeling and with conjugation to ^{14}C metformin. Metformin alone has poor bioavailability and was inhibited by the protein pump antagonist, omeprazole (Figure 5). ^3H and ^{14}C labeled QDs demonstrated a 7-fold greater uptake than metformin alone and was inhibited using a nonspecific clathrin and macropinocytosis inhibitor (Figure 5). These data corroborate the fluorescent data and demonstrate that uptake is promoted by endocytosis pathways.

Oral absorption of nanomaterials over the short time frame that we examined has not previously been reported. Furthermore, we have shown that our QDs are taken up by the liver and then cleared over a 24 h period by biliary excretion. Ag NPs of a similar size (6.7 nm) have previously been reported to have a limited bioavailability within blood at 10 min and 2 h.[25] Our results indicate that Ag_2S QDs have poor systemic bioavailability but are absorbed by the small intestine and taken up by the liver, then cleared by biliary excretion. The lack of systemic bioavailability reported by others[25] is likely to be a consequence of extensive first pass uptake by the liver.[26] Following on from this, we examined whether the selective uptake of QDs by LSECs and hepatocytes in the liver could be optimized with biopolymer coatings.

Liver Targeting Properties of Gavaged Ag_2S QDs Are Optimized by Biopolymer Coating. Given the increase in hydrodynamic diameter between our control uncoated QDs (30 nm) and biopolymer coated QDs (60 nm), an additional control QD coated with BSA was included. BSA was selected because QDs attach to this molecule *in vivo*, as shown in the results in Figure 2. QD-BSA demonstrated a 68.4 ± 3.2 hydrodynamic diameter and was radiolabeled in the same manner as the other biopolymer QDs.

A. Uptake of ^{14}C metformin, ^3H-QDs, QD-^{14}C metformin, ^3H oleic acid in small intestine explants following 1 hr incubation with/without endocytosis inhibitor pre-incubation

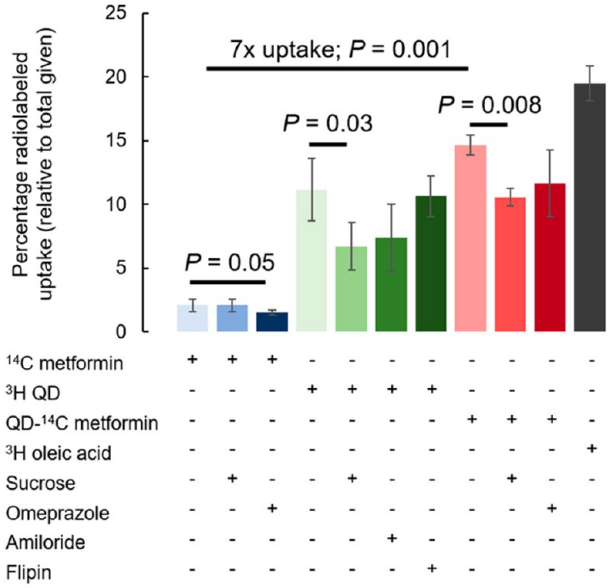

B. Inhibitors and endocytosis pathways blocked

Inhibitor	Clathrin	Caveolae	Macropinocytosis	OCT1 transporter
Sucrose	Blocks	-	Blocks	-
Omeprazole	-	-	-	Blocks
Amiloride	-	-	Blocks	-
Filipin	-	Blocks	-	-

Figure 5. Small intestine explant endocytosis of metformin and QDs. (A) 100 mg of explants of the small intestine were incubated with ^{14}C metformin with/without conjugation to QDs in the presence of endocytosis inhibitors for 1 h. (B) Summary table of inhibitor pathways. Metformin uptake was increased when conjugated to QDs *via* clathrin and macropinocytosis pathway.

60% of uncoated QDs labeled with ^3H accumulated in the liver within 30 min of an oral dose of 100 μL of 1 mM QDs (Figure 6A). QD-BSA showed no demonstrable any differences in biodistribution compared to uncoated QDs (Figure 6A). There was an increase to 85% liver targeting by coating the QDs in FSA (Figure 6A). Coating with heparin or gelatin did not increase radioactivity accumulation in the liver compared to uncoated QDs, however both demonstrated a wider biodistribution with greater uptake into the kidney and spleen, suggesting that these coatings may increase systemic bioavailability of QDs (Figure 6A). Extensive first pass uptake by the liver after oral dosing reduces systemic exposure and adverse effects, however limits the utility of these Ag_2S QDs to therapies or theranostics targeting the liver.

Cellular Biodistribution of QDs with Biopolymer Coating. We then determined whether any of the three different biopolymer coatings increased the uptake of QDs by LSECs, noting that these biopolymers are substrates for LSEC endocytosis.[4] Thirty min after administration of QDs by gavage, livers were perfused, and hepatocytes, LSECs, and KCs were isolated. Experiments were performed using QDs labeled with either ^3H-oleic acid or Alexa Fluor 488 TFP ester fluorescent tags (Figure 4). Comparison of the radioactivity levels in isolated cell types in the liver showed that 20% of uncoated QDs accumulated in LSECs *versus* 35% in hepatocytes (Figure 6B). BSA coating demonstrated the

https://dx.doi.org/10.1021/acsnano.9b06071
ACS Nano 2020, 14, 1492−1507

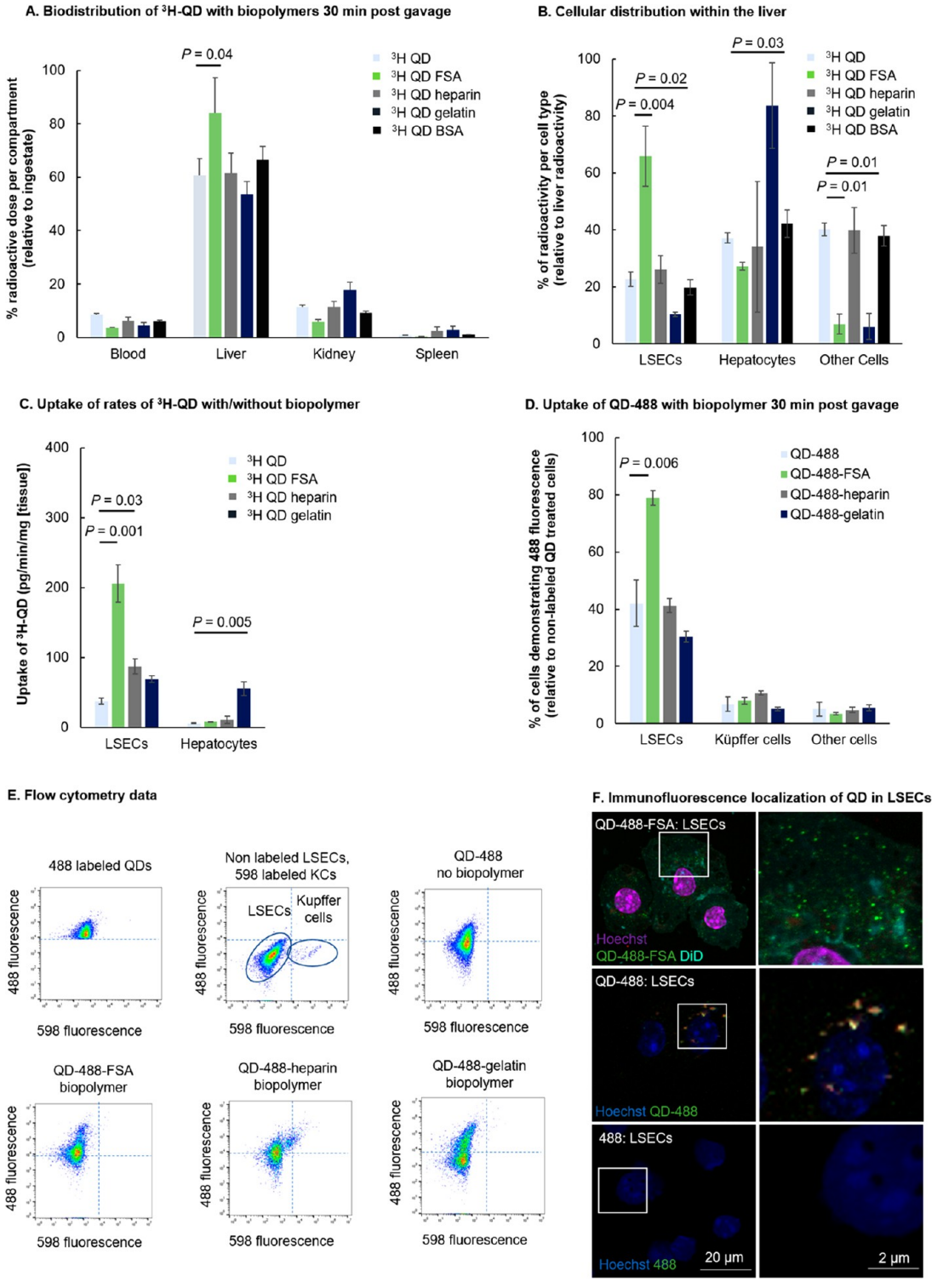

Figure 6. Liver accumulation and cellular targeting of Ag_2S QDs. (A−C) 100 μL of 1 mM radiolabeled ^{3}H-QD with/without biopolymer coating was orally administered to young mice. Thirty min later, blood, organs, and cell samples were collected and digested and radioactivity was detected. (A) The percentage of radioactivity relative to the ingestive for selected organs is shown. (B) Of the radiation observed in the liver, the percentages observed in LSECs, hepatocytes, and unknown cells are shown for QDs with/without biopolymer. (C) Picogram uptake of ^{3}H-QDs into LSECs and hepatocytes per mg of tissue per minute from blood. (D−F) 100 μL of 1 mM QD with an Alexa Fluor 488 TFP ester fluorescent tag was gavaged in young mice. Thirty min later, nonparenchymal liver cells were isolated (LSECs and KCs). KCs were stained with F4/80 conjugated with a 598 nm fluorescent tag, and cells were examined by flow cytometry. (D) The percentage of cells demonstrating 488 nm florescence following QD treatments with various polymers. (E) Representative raw data from flow cytometry. Panels show log scales of 488 and 598 detection. From left to right, panels show QD-488 alone, non-QD treated LSECs and KCs (KCs show 598 fluorescence), QD-488, QD-488-FSA, QD-488-heparin, and QD-488-gelatin. (F) Sample images of LSECs isolated following gavage treatments with QD-FSA-488, QD-488, and 488 TFP ester alone. Accumulation of 488 fluorescent tag is shown in LSECs.

https://dx.doi.org/10.1021/acsnano.9b06071
ACS Nano 2020, 14, 1492−1507

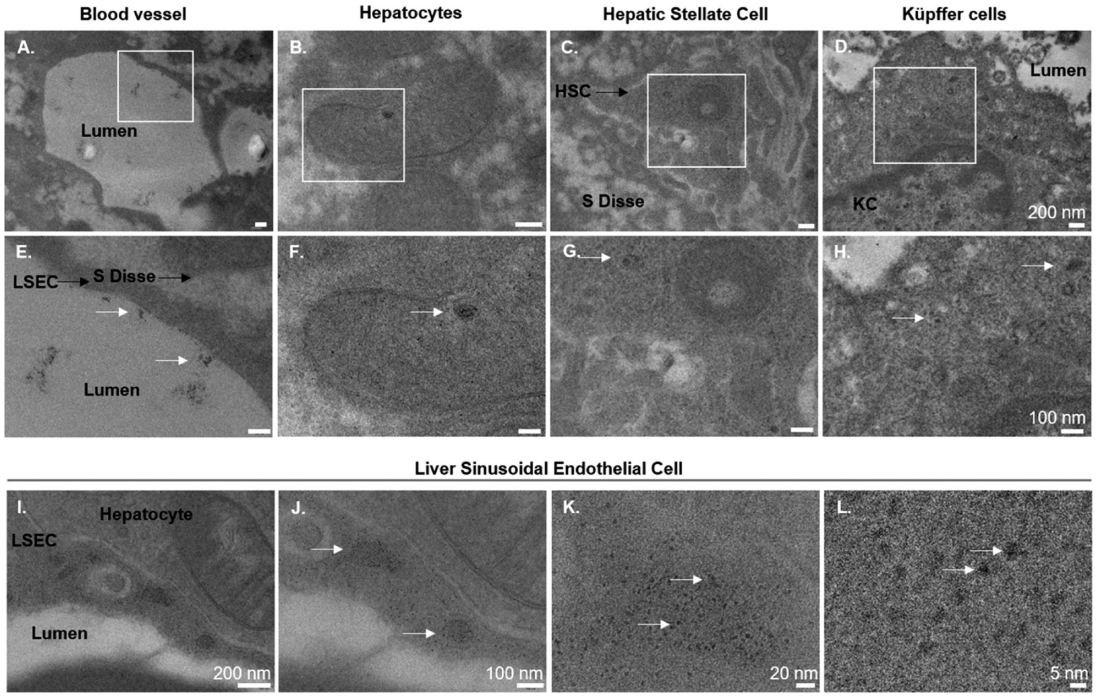

Figure 7. Transmission electron microscopy of intact livers 2 h following oral administration of QDs. Top row (A–D) shows sample images, and middle row (E–H) shows enlarged images from the top panel; Scale bars: top panels, 200 nm; middle panel, 100 nm. (A, E) Sinusoidal lumen showing clusters of QDs on the surface of LSECs lining the lumen (white arrows). Representative image of hepatocytes (B, F), hepatic stellate cells (HSCs) (C, G), and KCs (D, H) show minimal QD accumulation in these cell types. (I–L) LSECs demonstrate accumulation of QDs within the cytosol. These QDs appear to cluster together; however at high magnification, they appear not to be aggregating inside the cell.

same liver cell distribution as uncoated QDs (Figure 6B). FSA coating of QDs significantly increased LSEC targeting 3-fold and greatly reduced uptake by nonhepatocyte/LSEC cell types in the liver (Figure 6B). Gelatin coating greatly increased hepatocyte targeting with 85% of total radioactivity found in hepatocytes and 10% in LSECs and a reduction in the radioactivity of nonhepatocyte/LSEC cell types in the liver (Figure 6B). The uptake of radiolabeled FSA and gelatin QDs into LSECs and hepatocytes, respectively, from blood were increased compared to uncoated QDs (Figure 6C).

Flow cytometry analysis demonstrated that LSECs had the greatest accumulation of fluorescently labeled QDs. Following administration of uncoated QDs, 40% of LSECs contained a 488 fluorescent tag compared with 30% of KCs and 20% of other cells (HSCs or immune cells nonlabeled with F4/80) (Figure 6D,E). FSA coating led to increased targeting of LSECs in these flow cytometry studies with 75% of LSECs containing fluorescent tags and less uptake by KCs and other cells (Figure 6D,E). Mice gavaged with the Alexa Fluor 488 TFP ester alone did not show any 488 signals in isolated LSECs (Figure 6F).

TEM imaging of intact livers from 2 h post-gavage mice revealed QDs were present in the sinusoidal lumen, but there were only minimal numbers of QDs in hepatocytes, hepatic stellate cells, and KCs (Figure 7A–H). QD accumulation was predominantly compartmentalized to LSEC (Figure 7I–L), confirming the results of the radiolabeling and flow cytometry studies.

After administration by oral gavage, between 60 and 85% of the dose of Ag_2S QDs was taken up by the liver. Of the QDs sequestered in the liver, between 10 and 60% were found within LSECs, depending upon the biopolymer coating. FSA proved to be the best biopolymer for both targeting the liver and the LSEC. This is not surprising given FSA is avidly endocytosed by LSECs. Moreover, flow cytometry showed that the majority of LSECs were fluorescent after administration of Alexa Fluor 488 TFP ester bound QDs with an FSA coating. Together these results indicate that Ag_2S QDs coated with FSA are highly selective for LSECs and thus can provide specific targeting of LSECs for therapeutic or bioimaging purposes or for studies of LSEC biology. Another substrate for LSEC endocytosis is hyaluronic acid. Bhang *et al.*[27] previously found that QDs bound to hyaluronic acid targeted LSECs after intravenous injection. Thus, endocytosis receptors on the LSEC appear to be a reliable target for QD uptake.

Delivery of ^{14}C Metformin to the LSEC by QDs. To examine the ability of QDs and QD-FSA to transport therapeutic agents to the LSEC, we conjugated ^{14}C metformin to the QDs. These double radiolabeled QDs were uncoated or coated in FSA biopolymer. The bioavailability of oral metformin in humans is 40–60% under fasting conditions.[28] In mice, nonfasted metformin uptake is between 20 and 30% and is slowly absorbed into the blood.[29] Initially we examined ^{14}C-metformin biodistribution 2 h after oral dose. 25% of the dose was systemically bioavailable, with 10% uptake by the liver and <1% within LSECs (Figure 8A). FSA coating increased the bioavailability of metformin 3-fold in blood and 5-fold in the liver and increased LSEC uptake by 50-fold (Figure 8B,C). Treatment of mice with metformin bound to QDs did not alter liver function tests (AST, ALT) (Figure 8D). Comparing the distribution of ^{3}H and ^{14}C radiation confirmed that QDs and metformin remain conjugated during the passage through the small intestine into the LSECs (Figure 8E). We previously found that metformin influences the

https://dx.doi.org/10.1021/acsnano.9b06071
ACS Nano 2020, 14, 1492–1507

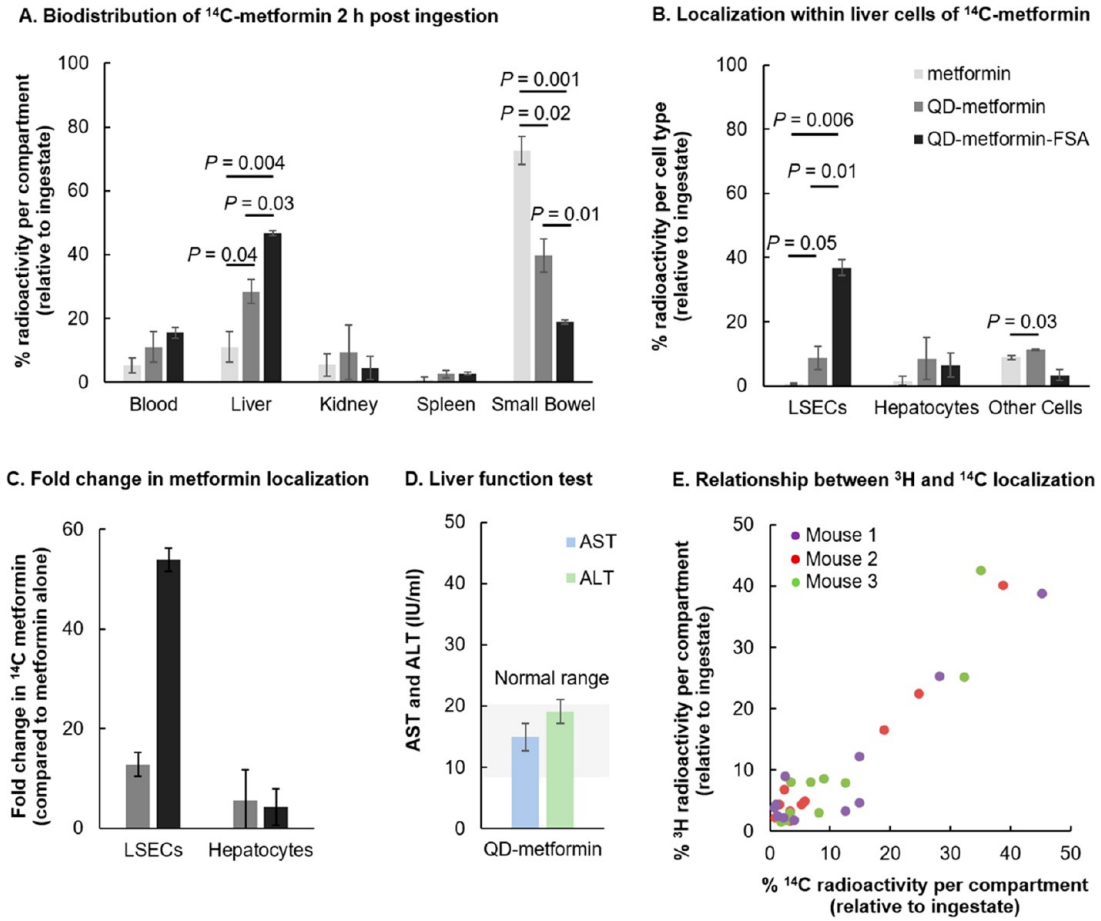

Figure 8. Biodistribution and targeting of LSEC of 14C-metformin is improved due to QD transportation 2 h post-oral administration. (A) Biodistribution of radiolabeled (i) metformin alone, (ii) metformin bound to QDs, and (iii) metformin bound to QDs with biopolymer coating (FSA). (B) Metformin localization within liver cells is increased by conjugation to QDs. (C) Fold change in metformin accumulation with QD and QD-FSA conjugation with metformin. (D) Liver function tests (AST and ALT). (E) Individual data points from mice 1, 2, and 3 showing the % ^{3}H and % ^{14}C radioactivity for each tissue sample examined. (F) phosphorylated AMPK and AMPK were quantified in isolated LSECs and hepatocytes 2 h following gavage. Increased pAMPK/AMPK ratios were observed compared to untreated and QD treated animals.

ultrastructure of LSECs, particularly reversing some of the age-related changes such as loss of fenestrations.[17] Conjugation of metformin to QDs increases the targeting of LSECs and raises the possibility of specifically improving LSEC function without systemic effects.

Endocytosis of QDs. Accumulation of QDs within LSECs may occur by multiple pathways, and we investigated these with the use of the SK-Hep1 cell line.[30] Visualization of endocytosis was performed using QDs conjugated to Alexa Fluor 488 TFP ester (Figure 9A). Visualization of monodispersed QD endocytosis was not possible due to the <10 nm sizing of QDs. However, incubation with FCS promotes aggregation and clustering of QDs that can be observed to be endocytosed (Figure 9A). QDs interacted with the cell membrane, attached to the cells (Figure 9A, white circles), and then migrated within the cells. Quantification of cellular endocytosis was performed using ^{3}H radiolabeled QD and QD-FSA. Incubation for 2, 4, and 24 h demonstrated that endocytosis occurred at similar rates for QD and QD-FSA (Figure 9B,C). Endocytosis *via* clathrin-mediated, caveolae-mediated, and pino-endocytosis pathways was inhibited by pre-incubation with specific inhibitors (filipin, amiloride, and sucrose, respectively). Inhibitor treatment demonstrated that caveolae-dependent endocytosis is critical for the endocytosis of FSA coated QDs over 24 h. On the other hand, uncoated QDs were endocytosed by several pathways. Uptake of uncoated QDs was inhibited by all treatments at all time points examined (Figure 9B). Uptake of FSA coated QDs was only inhibited by filipin, a specific inhibitor of caveolae-mediated endocytosis (Figure 9C).

Caveolae invaginations are structures <200 nm in diameter.[31] Particle size has been shown to dictate the endocytosis pathways used for the uptake nanobeads.[32] Larger particles (200−500 nm) were taken up by caveolae-dependent endocytosis, while smaller particles (50−100 nm) were taken up by clathrin-mediated endocytosis.[32] The hydrodynamic diameters of the uncoated and FSA coated QDs were 30 and 70 nm, respectively (Table 1). Therefore, the preferential endocytosis of QD-FSA by caveolae is probably a result of the larger hydrodynamic radius.

Conjugation of QDs with ^{14}C metformin demonstrated that cellular uptake of this drug can be improved by nanotechnology-based delivery pathways. Metformin alone has poor uptake into SK-Hep1 cells with a 35-fold increase in uptake following conjugation with QDs (Figure 9D).

https://dx.doi.org/10.1021/acsnano.9b06071
ACS Nano 2020, 14, 1492−1507

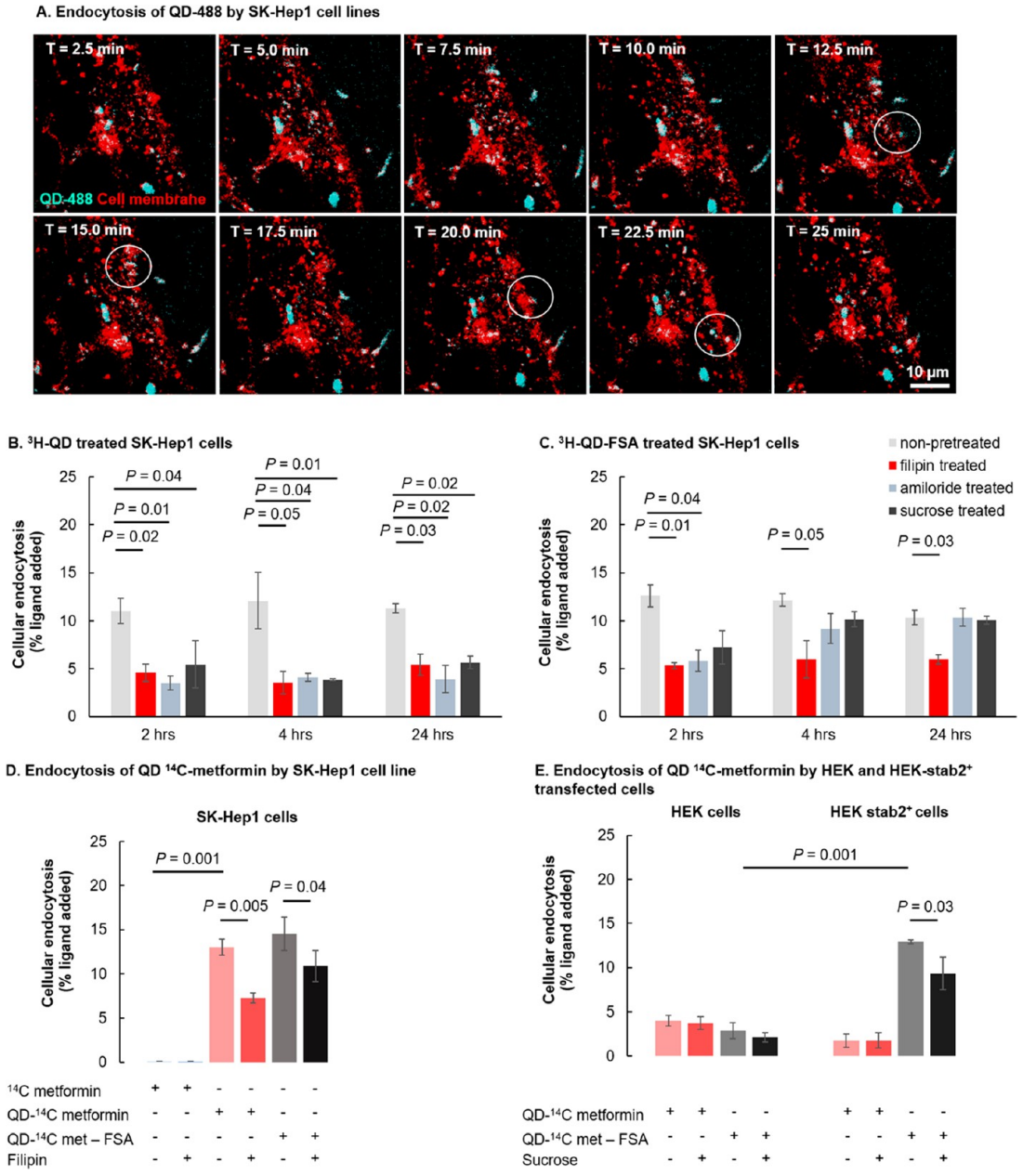

Figure 9. Endocytosis and toxicity of QDs in the SK-Hep1 cell line. (A) Time lapse imaging of SK-Hep1 cells stained with the membrane stain DiD (red) following incubation of QDs with bound Alexa Fluor 488 TFP ester (turquoise). Samples are incubated with FCS to promote aggregation of QDs to observe interaction with the cell membrane. White circles show point of interaction between QD-488 and the cell membrane prior to endocytosis. (B–D) Cellular endocytosis was determined based on the accumulation of ^{3}H-QDs within SK-Hep1 cells relative to the % of radioactive ligand given. Following treatment with 1 mM QDs for 2, 4, and 24 h, the media was removed, and cells were washed. Cells were lysed, and the cellular material was collected. (B) Cellular endocytosis of QDs without biopolymer was inhibited by various pretreatments. (C) Cellular endocytosis of QD-FSA was inhibited by filipin pretreatment alone. (D) ^{14}C metformin with and without conjugation to QDs and QD-FSA in SK-Hep1 cells. Conjugation with QDs increased metformin uptake by 35-fold with inhibition by filipin pretreatment. (E) Endocytosis of ^{14}C metformin in HEK cells and HEK cells transfected with stabilin-2 overexpression. Stabilin-2 overexpression increased FSA polymer coated QD-metformin uptake.

To better understand the receptors involved in QD-FSA uptake, HEK cells transfected with stabilin-2 receptor overexpression were examined. HEK cells have minimal uptake of QD-metformin and QD-metformin with FSA biopolymer coating (Figure 9E). Transfection with stabilin-2 receptor increased FSA coated QD uptake into the HEK cells to similar levels observed in SK-Hep1 cells, however had no effect on the uptake on uncoated QDs. This suggests that the stabilin-2 receptor and receptor-mediated endocytosis are key mediators in QD-FSA uptake.

Following cellular uptake in SK-Hep 1 cells, QDs colocalize in lysosomes (Figure 10A). Time lapse imaging demonstrates that QD-488 fluorescence intensity decreases with elevated Lysotracker staining expression (Figure 10B). SK-Hep 1 cells incubation of QDs (250 μg/mL) with/without FSA biopolymer coating and inhibitor treatments for 2, 4, and 24 h in serum-free media did not show any toxicity (Figure 10C).

https://dx.doi.org/10.1021/acsnano.9b06071
ACS Nano 2020, 14, 1492–1507

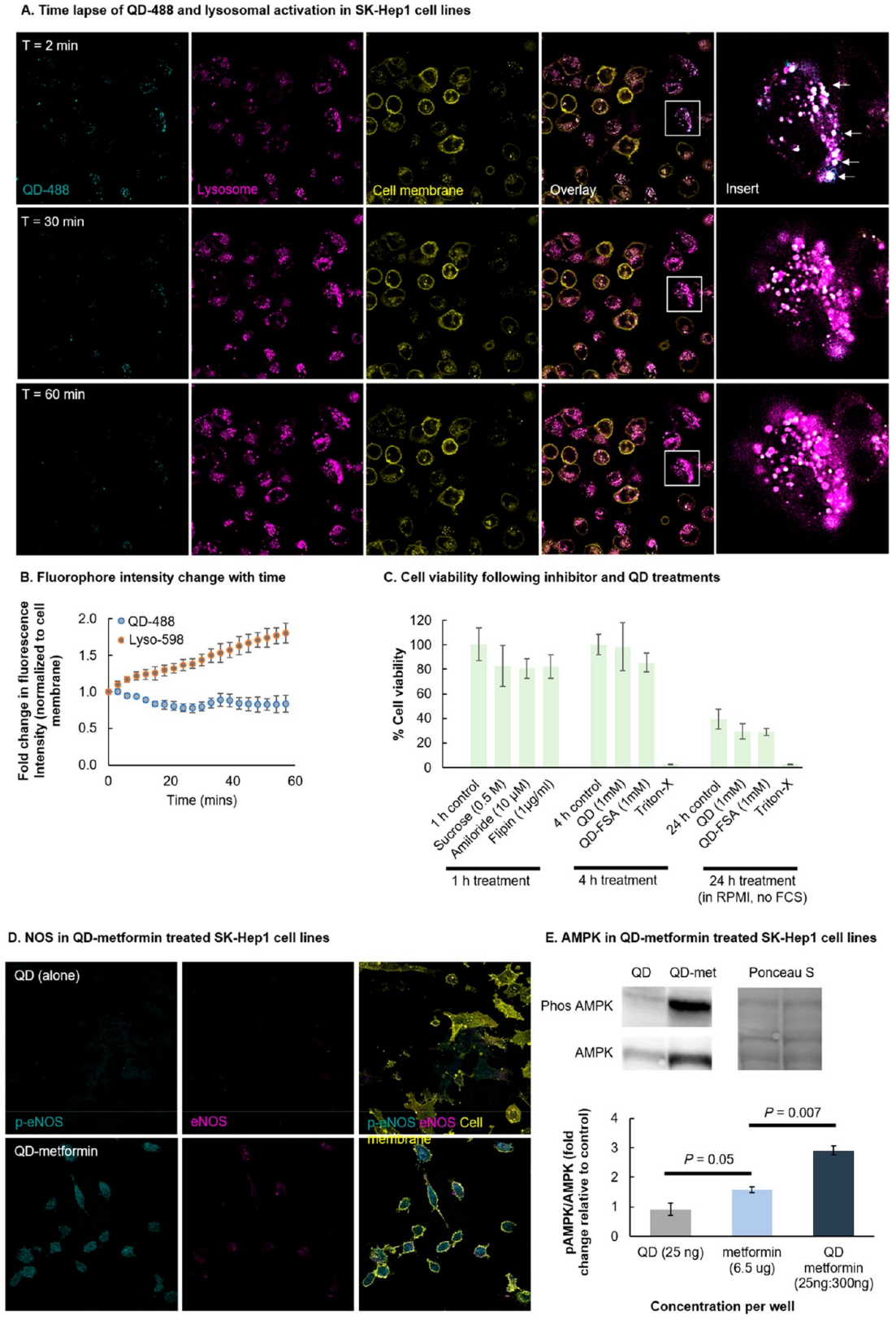

Figure 10. Lysosomal degradation and effects of QD-metformin on nitric oxide and AMPK. (A) Time lapse imaging of SK-Hep1 cells stained with the membrane stain DiD (yellow), lysotracker red (purple), following incubation of QDs with bound Alexa Fluor 488 TFP ester (turquoise). Samples are not incubated with FCS. White dots show colocalization with QDs and lysosomes. (B) Fluorophore intensity over time shows increased lysosome and decreased QD-488. (C) SK-Hep1 cell viability is not effected by inhibitor pretreatments or QD incubations for 4 or 24 h. (D, E) Sk-Hep1 cell times were incubated with 25 ng Ag_2S conjugated with 300 ng metformin for 2 h. Cells were fixed and stained for phosphorylated endothelial NOS (p-eNOS) and eNOS. Phosphorylated AMPK and AMPK were quantified by Western blot and demonstrated a 3-fold increase in expression ratios compared to untreated cells. Higher dosage metformin treatment demonstrated lower pAMPK/AMPK activation.

https://dx.doi.org/10.1021/acsnano.9b06071
ACS Nano 2020, 14, 1492−1507

Ag_2S QDs with 2-mercaptopropionic acid coating have previously also been shown to be nontoxic *in vitro* (IC: 50−1000 μg/mL).[33]

Finally, QD-metformin was found to induce biological effects in SK-Hep1 cells following 2 h of treatment. Twenty-five ng QDs conjugated with 300 ng metformin promoted increased expression of phosphorylated eNOS and eNOS compared to QD treated cells (Figure 10D). Phosphorylated AMPK and AMPK were quantified using Western blot and demonstrated a 3-fold increase in pAMPK to AMPK ratios (Figure 10E). Comparatively, a 20-fold higher dosage of metformin promotes a 50% less change in pAMPK/AMPK. This effect highlights the effects of QDs on the cellular uptake of metformin.

CONCLUSION

We have demonstrated targeted delivery of Ag_2S-based QDs with bound materials to the LSECs *in vitro* and *in vivo* following oral administration. These QDs rapidly transfer across the small intestine *via* clathrin- and micropinocytosis-mediated pathways. 60% of an oral dose of QDs was rapidly distributed to the liver within 30 min, and this increased to 85% with FSA biopolymer coating. Of these QDs in the liver, uptake by LSECs also increased from 25% to 75% with FSA coating, while uptake into hepatocytes was increased from 40% to 85% with gelatin coating. Overall, 85% of ingested QDs were cleared within 24 h of administration *via* the faeces with limited biodistribution into other organs. The bioavailability of ^{14}C-metformin 2 h post-ingestion in the liver was increased by 5-fold by conjugation with QD-FSA, while uptake of metformin into LSECs was increased 50-fold with these QDs. Endocytosis of QDs was inhibited by sucrose and filipin, indicating that QD uptake is regulated by clathrin- and caveolae-mediated pathways. In conclusion, we have shown high specificity targeting of the LSEC or hepatocytes after oral administration of QDs coated with a biopolymer layer of FSA or gelatin, which improved the bioavailability and delivery of metformin to LSECs.

EXPERIMENTAL PROCEDURES

Ethics. The study was approved by the Animal Welfare Committee of the Sydney Local Health District and was performed in accordance with the Australian Code of Practice for the care and use of animals for scientific research (AWC approval: 2018/010). All information provided accords with the ARRIVE guidelines.

Materials. Silver diethyldithiocarbamate (cat. no.: D93503, Merck, AUS), 1-dodecanethiol (cat. no.: 471364 Merck, AUS), cyclohexane (Merck, AUS) acetone (Merck, AUS), N_2 gas (BOC, AUS), Ar gas (BOC, AUS), 3-mercaptopropionic acid [3-MPA] (cat. no.: M5801, Merck, AUS), ^{14}C-metformin (cat. no.: MC-2023, Moravek, USA), ^{3}H oleic acid (cat. no.: O-1518, Merck, AUS), gelatin (cat. no.: G-9392 Merck, AUS), heparin (cat. no.: H1027, Merck, AUS), *N*-(3-(dimethylamino)propyl)-*N*′-ethyl carbodiimide hydrochloride [EDC] (cat. no.: E6383 Merck, AUS), *N*-hydroxysulfosuccinimide sodium salt [NHS] (cat. no.: 56485, Merck, AUS), adipic acid dihydrazide (cat. no.: A0638, Merck, AUS), SnakeSkin dialysis tubing 10,000 MWCO (cat. no.: 88243, ThermoFisher Scientific, AUS), scintillation fluid (Ultima Gold 2×, cat. no.: 6013329, PerkinElmer, AUS), 30% H_2O_2 (cat. no.: 18312, Merck, AUS), solvable solution (cat. no.: 6NE9100, PerkinElmer, AUS), collagenase (type 1, cat. no.: 47D17410A, ProSciTech, AUS), RPMI-1640 (Merck, AUS), Percoll (Merck, AUS), DMEM (Gibco Invitrogen, Melbourne, Australia), penicillin-streptomycin (Merck, AUS), fetal calf serum (Merck, AUS), *in Vitro* Toxicology Assay Kit, MTT based (cat. no.: TOX1-1KT, Sigma-Aldrich, AUS), antimouse F4/80 (cat. no.: MF48000, ThermoFisher Scientific, AUS), *p*-AMPKα (Thr172, cat. no.: 2531, Cell Signaling Technology, AUS), AMPKα (cat. no.: 2532, Australian Biosearch, AUS), anti-p-eNOS (Ser1177, cat. no.: 9571, Genesearch, AUS), anti-eNOS (type 3, cat. no.: 610296, BD Bioscience, AUS), Alexa Fluor 488 goat anti-rabbit (cat. no.: R-37116; Thermo Fisher AUS), Alexa Fluor Cy3 goat anti-mouse (cat. no.: A-10521; Thermo Fisher, AUS) Alexa Fluor 488 goat anti-rabbit (cat. no.: R-37116; Thermo Fisher, AUS), goat anti-mouse Alexa Fluor 594 (cat. no.: A-11005, ThermoFisher Scientific, AUS), Alexa Fluor 488 TFP ester (cat. no.: A37570, ThermoFisher Scientific, AUS), TEM grids (cat. no.: 71150, Electron Microscopy Sciences, USA), Lyso Tracker Red DND-99 (cat. no.: L7528, ThermoFisher Scientific, AUS), DiD Cell-Labeling Solution (cat. no.: V22887, ThermoFisher, AUS), Hoechst 33342 (cat. no.: 14533, Merck, AUS), glass coverslips (cat. no.: 72230-01, Electron Microscopy Sciences, USA), Fluoromount-G (cat. no.: 00-4958-02 ThermoFisher, AUS), epoxy embedding medium kit (cat. no.: 45359, Merck AUS). Western blot reagents: Loading buffer (cat. no.: B0007, Thermo Fisher), running buffer (cat. no.: B0001, Thermo Fisher), transfer buffer (cat. no.: BT00061, Thermo Fisher), Ponceau staining (cat. no.: P7170, Sigma− Aldrich), PBS tablets (cat. no.: P4417, Sigma−Aldrich), and Tween-20 (cat. no.: P1379, Sigma−Aldrich).

Synthesis of Ag_2S QDs and NPs. Ag_2S QDs synthesis has previously been reported.[34,35] Ag_2S QDs were synthesized with 0.1 mM silver diethyldithiocarbamate with 12 mL of 1-dodecanethiol mixed under vigorous magnetic stirring.[35] A N_2 vacuum was created to remove oxygen from the mixture, followed by an Ar vacuum to remove N_2. The solution was heated to 200 °C at a rate of 12 °C per min and held at this temperature for 60 min. Following synthesis, EtOH was added to the solution followed by centrifugation. Ag_2S QDs were resuspended in minimal cyclohexane and washed twice with EtOH. Each wash resulted in precipitation of Ag_2S QDs and isolated with centrifugation.

NPs were produced using the same methods; however, the solution was heated to 135 °C and held at this temperature for 10 min. The solution was then cooled rapidly on an ice bath. Washing stages, phase transfer, and radiolabeling are described below.

Aqueous Phase Transfer. QDs in cyclohexane were mixed 1:1 (v/v) with acetone under magnetic stirring. One mL of 3-mercaptopropionic acid was added per 25 mg of Ag_2S QDs and mixed under magnetic stirring at room temperature for 1 h. Following this, QDs were mixed with EtOH and centrifuged. The pellet was redispersed in minimal MQ and washed with EtOH twice and dispersed in MQ. Samples were then filtered using Whatman grade 4 filter paper. QDs were diluted to 10 mM for storage at 4 °C in the dark.

Radiolabeling. Ten mM QDs were incubated at room temperature with 0.5 μCi ^{3}H oleic acid for 3 h in a sonication bath and 24 h under Ar gas with vigorous stirring. Removal of excess oleic acid was performed by two EtOH wash stages with centrifugation and redispersion in minimal MQ.

^{14}C metformin was conjugated to QDs *via* EDC/NHS coupling. One mM Ag_2S QD was mixed with 1 mM EDC and 1 mM NHS in a reaction vial under heavy mixing for 1 h. Following this, the pH was not altered, and 1.0 μCi ^{14}C metformin was added to the solution. The solution was mixed overnight and transferred to dialysis tubing 10,000 MWCO and dialyzed with 1 mL of solution per 1 L of PBS for 2 h, 5 h, and overnight at 4 °C in the dark.

Biopolymer Synthesis. FSA was produced as previously described by Mego *et al.*[36] Briefly, FSA was prepared by treating BSA with 10% formaldehyde in 0.2 M carbonate buffer, pH 10, for 3 days at room temperature with gentle stirring, followed by dialysis against PBS. One mg/mL gelatin was heated to 70 °C for 30 min and vortexed for 1 min. One mg/mL heparin was mixed for 5 min by vortexing.

Conjugation of biopolymers with an Alexa Fluor 488 TFP ester was performed using EDC/NHC coupling. One mg/mL FSA, GEL, or HEP was incubated with 1 mM EDC and 1 mM NHS in a reaction vial under heavy mixing for 1 h. Following this, the pH was increased to 9 using $NaCO_3$, and 1 mM Alexa Fluor 488 TFP ester was added

https://dx.doi.org/10.1021/acsnano.9b06071
ACS Nano 2020, 14, 1492−1507

to the solution. Heparin solutions had 1 mM adipic acid dihydrazide added to the mixture in addition to the 488 TFP ester. The mixture was incubated at room temperature for 4 h under mixing conditions. The mixture was transferred to dialysis tubing 10,000 MWCO and dialyzed with 1 mL of biopolymer solution per 1 L of PBS for 2 h, 5 h, and overnight at 4 °C in the dark.

QD Coated with Biopolymer. Ten mM Ag_2S QDs were mixed with 10 mM EDC and 10 mM NHS in a reaction vial under heavy mixing for 1 h. Following this, the pH was increased to 9 using $NaCO_3$, and 1 mg/mL fluorescent biopolymer (BSA, FSA-488, GEL-488, HEP-488) was added to the solution. QDs that were not coated with biopolymer had a fluorescent tag attached to its surface *via* the same methodology (EDC/NHS coupling with Alexa Fluor 488 TFP ester). The mixtures were incubated at room temperature for 4 h under mixing conditions. Removal of excess polymer was performed by two EtOH wash stages with centrifugation and redispersion in minimal MQ. The mixture was transferred to snakeskin dialysis tubing 10,000 molecular weight filters and dialyzed with PBS for 3 h, 5 h, and overnight at 4 °C in the dark. Following dialysis, solutions were collected from the tubing, centrifuged, redispersed at 10 mM, and stored at 4 °C until use.

Fourier Transformed Infrared Microscopy. Confirmation of the deposition on QDs was performed using FTIR. FTIR was performed on a LUMOS FTIR microscope (Bruker, USA) at the vibrational spectrometry facilities at Sydney Analytical, the University of Sydney. Samples were collected from dried QD or biopolymer solutions with a minimum of 10 measurements per material performed. Data show the average spectrum across 3500−700 nm in ATR mode, following atmosphere correction and normalization. Average spectrum was produced from 10 to 20 individual measurements per material.

ZetaSizer Characterization. Hydrodynamic diameter and ζ potential were measured using a Zetasizer Nano ZS (Malvern Bioanalytical, AUS), at the Bosch Molecular Biology Facility, the University of Sydney. Measurements were performed using 1 mM QDs in MQ in triplicate.

pH Stability. The pH solutions at 3, 5, 7, 9, and 11 were prepared using HCl and NaOH. QDs with fluorescent biopolymer (FSA-488, GEL-488, HEP-488) were incubated for 4 h at room temperature. QDs were centrifuged and redispersed in MQ. Fluorescence was measured using an EnSpire Multimode plate reader (PerkinElmer, AUS) and compared to diluted standards of QD with fluorescent biopolymer that did not undergo treatments. Data are presented as a percentage of remaining fluorescent in the sample following incubation. Incubation with pH 3 for 96 h was also performed with FTIR spectra collected. Spectra was collected as described above.

High-Voltage Transmission Electron Microscopy. Visualization of QDs from biological and nonbiological samples was performed using high-voltage transmission electron microscopy (HV-TEM). HV-TEM was performed on a JEOL 2100 (JEOL, AUS) at the transmission electron microscope facilities at the Australian Centre for Microscopy and Microanalysis, the University of Sydney. Nonbiological samples were prepared by evaporative deposition on carbon-based TEM grids. Biological samples were prepared as previously described.[17] Briefly, perfused liver sections were cut into 1 mm^3 cubes and fixed with 2.5% glutaraldehyde. Samples were then processed and embedded with epoxy resin following kit instructions. Resin blocks were sectioned using an ultrathin microtome Leica EM UC6 (Leica Microsystems, AUS) and mounted on TEM grids.

Mice Gavage. 3−4-month-old male C57/Bl6 mice were obtained from the Animal Resource Centre in Perth, Western Australia. Animals were housed at the ANZAC Research Institute animal house on a 12 h light/dark cycle and provided with *ad libitum* access to food and water. Mice were not fasted prior to gavage with either 100 μL of 1 mM (i) ^{3}H- or (ii) nonradiolabeled Ag_2S QDs with and without biopolymer coatings. Gavage was performed using an esophageal gavage needle and delivered in a single rapid dose. Mice were euthanized by a single intraperitoneal injection of 100 mg/kg ketamine and 10 mg/kg xylazine in saline at 30 min, 2 h, and 24 h post-gavage. 200−250 mg of tissue samples was collected from the liver, spleen, kidney, lung, and small bowel along with 100 μL of blood. Tissue samples were weighed and mixed in a reaction vial with 1 mL of solvable solution and incubated at 60 °C for 4 h to dissolve the tissue. 0.2 mL of 30% H_2O_2 was added to samples to reduce the dark color saturation. Samples were mixed with 10 mL scintillation fluid.

Small Intestine Explant Endocytosis. Explants were performed based on previous work by Danielsen *et al.*[24] The small intestine was removed and washed with ice cold RPMI media for 5 min. 100 mg small intestine segments were excised and placed in a 24 well plate with 1 mL of RPMI media. Samples were incubated at 37 °C for 15 min. Samples were then pre-incubated with endocytosis inhibitor treatments filipin (caveolae blocking; 1 μM, 45 min), amiloride 1 mM (micropinocytosis blocking; 1 mM, 45 min), sucrose (nonspecific clathrin and macropinocytosis blocking; 0.5 M, 30 min), and omeprazole (protein pump inhibitor; 10 μM, 30 min) in DMPI media without FCS. Explants were then washed with warmed PBS and incubated with either ^{14}C-metformin, ^{3}H labeled QDs, QD-^{14}C-metformin, or ^{3}H oleic acid for 1 h. The supernatant was removed, and the tissue was washed with warmed PBS. Tissue samples were dissolved using 1 mL of solvable solution and prepared as stated above for radiolabeled detection. All samples were performed in duplicate with three biological replicates.

LSEC Isolation. As per our previous studies,[17,18] hepatocytes, LSECs, and KCs isolation was performed by perfusion of the liver with collagenase. Hepatocytes were removed by three 10 min centrifugations at 50*g*. Nonparenchymal and dead cells were removed from the hepatocyte and LSEC fractions by separate two-step Percoll gradients with KCs either removed from the LSEC fraction by selective adherence to plastic (radiolabeled samples) or this step was not performed (flow cytometry analysis). Cells were suspended in PBS followed by cell counting, centrifuged and weighed, following either (i) mixing in a reaction vial with 1 mL solvable solution and prepared as stated above for radiolabeled detection or (ii) unaltered for analysis in flow cytometry (samples for flow cytometry were not radiolabeled).

^{3}H and ^{14}C Radiolabeled Activity Analysis. Radioactivity was measured using a scintillation counter (Tricarb 2100 TR, PerkinElmer, AUS). All samples were mixed with 10 mL of scintillation fluid (5 measurements per sample). Baseline measurements were collected from control mice that were not treated with radioactivity QDs. Data were collected as disintegrations per minute and used for analysis. All radioactivity data presented in this manuscript used n = 3 mice per group, and for SK-Hep1 endocytosis, the experiments were performed in triplicate.

Flow Cytometry. Flow cytometry was performed on a BD-Accuri flow cytometer (BD biosciences, AUS) with data analyzed on FlowJo (v10, FlowJo LLC, ON, USA). LSEC and KC mixed samples were diluted to 1.0 × 10^6 cells/mL, and additional serial half dilutions were also performed. Prior to flow analysis, KCs were labeled with F4/80 conjugated to Alexa Fluor 598. 100,000 events were collected per dilution with events limited to size criteria. Results show the sample data with a log10 scale following size execution with 488 signal (y axis) and 594 signals (x axis). All flow cytometry data presented in this manuscript used n = 3 mice per group.

Cell Culture. The human SK-Hep1 and HEK293T cells were obtained from the American Type Tissue Culture Collection (ATCC, Manassas, VA) and were cultured in a humidified 5% CO_2 incubator at 37 °C. Cells were grown in DMEM supplemented with 10% fetal calf serum and penicillin-streptomycin. Transfection with stabilin-2 receptor was performed previously as previously described.[37] Briefly, the cDNA of interest was inserted into a pEF6/V5-His-TOPO vector followed by blasticidin (Calbiochem, Merck, Germany) and stably transfected in HEK293T cells.

Endocytosis. Endocytosis of ^{3}H-QDs with and without FSA biopolymer, ^{14}C-metformin, QD-^{14}C-metformin with and without FSA biopolymer was performed using the SK-Hep1, HEK, and stab-2 transfected HEK cell lines.

Cells were plated at 0.125 × 10^6 cells in a 24-well plate with DMEM media supplemented with 10% FCS. Twenty-four h following

https://dx.doi.org/10.1021/acsnano.9b06071
ACS Nano 2020, 14, 1492−1507

plating, cells were starved of FCS for 4 h before use. Cells were pretreated with inhibitors of endocytotic pathways: filipin (caveolae blocking; 1 μM, 45 min), amiloride 1 mM (micropinocytosis blocking; 1 mM, 45 min), sucrose (nonspecific clathrin and micropinocytosis blocking; 0.5 M, 30 min), or omeprazole (10 μM, 30 min) in DMPI media without FCS. SK-Hep 1 cells were then incubated with 500 μL of 1 μM ^{3}H-QD with or without FSA coating for 2, 4, and 24 h in DMPI without phenol red. SK-Hep 1, HEK, and stab-2 transfected HEK cells were incubated with 500 μL of 1 μM ^{14}C-metformin, QD-^{14}C-metformin with and without FSA biopolymer for 2 h in DMPI without phenol red.

Following incubation, two fractions were collected of cell media and lysed cells. Cell media was collected with a subsequent 500 μL of PBS wash. Cells were then lysed with 500 μL of 0.1% SDS solution and collected using a cell scraper, and wells were washed with 500 μL of PBS with the rinse solution collected. Radioactivity was measured using a scintillation counter (Tricarb 2100 TR, PerkinElmer, AUS). The proportion of radiation relative to the total injectate is shown. All radioactivity studies were performed in triplicate.

Cell Viability Assays. MTT assays performed as instructed by the kit manufacturer following inhibitor treatments of SK-Hep1 cells. Cells were washed with PBS and incubated with RPMI media containing 100 μg MTT solution. Cells were incubated at 37 °C for 4 h and lysed with 200 μL of solubilization solution, and after 30 min, absorbance was measured at 570 nm using a spectrophotometer. For SK-Hep1 cell viability, the experiments were performed in triplicate.

Western Blots. SK-Hep1 cells were starved for 4 h by removing FCS from DMEM media. Cells were treated with 25 ng/mL QDs, 25 ng/mL QDs conjugated with 300 ng/mL metformin, and 6.5 μg/mL metformin for 2 h. Cells were lysed, and total protein was extracted as previously described.[17] Bolt tris-bis plus gels were run. After transfer, the PVDF membrane was incubated with primary antibodies (p-AMPK, AMPK) followed by incubation with secondary antibody (antirabbit and antimouse) and developed using ECL-Plus chemiluminescence detection solution. Percentages of density were obtained by normalizing to the control. Densitometry measurements were performed using ImageJ software. Mean ± SD was calculated from 3 to 4 individual experiments.

Confocal and Live Microscopy. Confocal imaging of *in vitro* SK-Hep1 cells was performed on a Leica SP8 (Leica Microsystems, AUS). SK-Hep1 cells were starved for 4 h by removing FCS from DMEM media. Cells were treated with 25 ng/mL QDs and 25 ng/mL QDs conjugated with 300 ng/mL metformin. Primary antibodies (1:100) to phosphorylated eNOS and eNOS were incubated overnight at 4 °C and conjugated secondary antibodies (1:200) Alexa Fluor 488 goat antirabbit or Alexa Fluor Cy3 goat antimouse and stained with DiD (1:200, 20 min), Hoechst 33342 (1:1000, 15 min). Coverslips were mounted on glass slides using Fluoromount-G. Imaging was performed using HyD detectors (Leica Microsystems, AUS) at 63× magnification with image analysis performed using LAS software (Leica Microsystems, AUS), Huygens Deconvolution software (Scientific Volume Imaging, Netherlands), and ImageJ (National Institute of Health, USA).

Live imaging of SK-Hep1 cells was performed using cells plated on glass coverslip dishes 14 mm microwell of 35 mm glass-bottom dishes (MatTek, USA). These cells were stained with Lyso Tracker Red DND-99 for 30 min and/or DiD for 20 min, washed with PBS, and imaged using HyD detectors attached to the Leica SP8. Incubation of SK-Hep1 cells was performed at 37 °C with 5% CO_2 for 1−2 h with 1 μM QD-488 using an EVOS on-stage incubator (ThermoFisher, AUS).

Wide-field imaging of *in vivo* small intestine tissue was performed using a 3i VIVO Spinning Disk IntraVital Confocal microscope (3i, USA). Mice were gavaged with 100 μL of 1 mM Ag_2S QDs coupled with Alexa Fluor 488 TFP ester and then anesthetized with a single intraperitoneal injection with 100 mg/kg ketamine and 10 mg/kg xylazine. Once anesthetized (3−4 min), the small intestine was exposed by an incision on the right side of the abdomen. The intestine was extended into a dish containing warmed PBS. Live imaging was performed using DAPI and FITC channels over a 30 min period (the DAPI channel was observed to collect refractive light as opposed to fluorescence). Images of the small intestine and mesenteric vein were collected. Image analysis was performed using SlideBook software and ImageJ software (National Institute of Health, USA).

Statistics. Statistical analysis comparing multiple groups was performed using Kruskal−Wallis tests with a *post hoc* Dunn's method (SPSS v22, IBM, USA). All radioactivity and flow cytometry data presented in this manuscript used $n = 3$ mice per group, and for SK-Hep1 endocytosis and cell viability, the experiments were performed in triplicate.

AUTHOR INFORMATION

Corresponding Author

Victoria C. Cogger − *ANZAC Research Institute and Aging and Alzheimer's Institute and Centre for Education and Research on Ageing, Concord Repatriation General Hospital, Concord 2139, Australia; Faculty of Medicine and Health and Charles Perkins Centre, The University of Sydney, Sydney 2006, Australia;* orcid.org/0000-0002-6346-9928; Email: victoria.cogger@sydney.edu.au

Authors

Nicholas J. Hunt − *ANZAC Research Institute and Aging and Alzheimer's Institute and Centre for Education and Research on Ageing, Concord Repatriation General Hospital, Concord 2139, Australia; Faculty of Medicine and Health and Charles Perkins Centre, The University of Sydney, Sydney 2006, Australia;* orcid.org/0000-0002-9001-0602

Glen P. Lockwood − *ANZAC Research Institute and Aging and Alzheimer's Institute and Centre for Education and Research on Ageing, Concord Repatriation General Hospital, Concord 2139, Australia; Charles Perkins Centre, The University of Sydney, Sydney 2006, Australia*

Frank H. Le Couteur − *ANZAC Research Institute, Concord Repatriation General Hospital, Concord 2139, Australia*

Peter A. G. McCourt − *Charles Perkins Centre, The University of Sydney, Sydney 2006, Australia; Department of Medical Biology, University of Tromsø - The Arctic University of Norway, Tromsø 9037, Norway*

Nidhi Singla − *Nano Institute, The University of Sydney, Sydney 2006, Australia*

Sun Woo Sophie Kang − *ANZAC Research Institute and Aging and Alzheimer's Institute and Centre for Education and Research on Ageing, Concord Repatriation General Hospital, Concord 2139, Australia; Faculty of Medicine and Health, The University of Sydney, Sydney 2006, Australia*

Andrew Burgess − *ANZAC Research Institute, Concord Repatriation General Hospital, Concord 2139, Australia; Faculty of Medicine and Health, The University of Sydney, Sydney 2006, Australia*

Zdenka Kuncic − *Charles Perkins Centre, School of Physics, and Nano Institute, The University of Sydney, Sydney 2006, Australia*

David G. Le Couteur − *ANZAC Research Institute and Aging and Alzheimer's Institute and Centre for Education and Research on Ageing, Concord Repatriation General Hospital, Concord 2139, Australia; Faculty of Medicine and Health and Charles Perkins Centre, The University of Sydney, Sydney 2006, Australia*

Complete contact information is available at: https://pubs.acs.org/10.1021/acsnano.9b06071

Author Contributions

The study concept was completed by V.C., D.L.C., Z.K., and P.G. The experimentation was completed by N.H., G.L., F.L.C., N.S., S.K., and A.B. The figures were completed by

https://dx.doi.org/10.1021/acsnano.9b06071
ACS Nano 2020, 14, 1492−1507

N.H. The manuscript was written by N.H., V.C., D.L.C., Z.K., and P.G.

Notes

The authors declare no competing financial interest.

ACKNOWLEDGMENTS

NHMRC project grants: no. 1141234; Sydney Medical School Foundation McKnight Bequest, The University of Sydney DVCR Research Equity Fellowship, The University of Sydney Seed Grant, and the University of Tromsø Faculty of Health Sciences travel grant to P.M. The Bosch Molecular Biology Facility, H. Lei and the Australian Centre for Microscopy and Microanalysis, E. Carter, J. Lee and the Sydney Analytical Vibrational Spectrometry Facility, the University of Sydney. M. Kockx and the Atherosclerosis group, and the Microscopy and Flow Cytometry Core Facility, ANZAC Research Institute. Concord RG Hospital Electron Microscopy Unit. Christopher Holte, University of Tromsø, Norway.

REFERENCES

(1) Chan, W. C.; Nie, S. Quantum Dot Bioconjugates for Ultrasensitive Nonisotopic Detection. *Science* **1998**, *281*, 2016−2018.
(2) Bruchez, M.; Moronne, M.; Gin, P.; Weiss, S.; Alivisatos, A. P. Semiconductor Nanocrystals as Fluorescent Biological Labels. *Science* **1998**, *281*, 2013−2016.
(3) Tsoi, K. M.; MacParland, S. A.; Ma, X.-Z.; Spetzler, V. N.; Echeverri, J.; Ouyang, B.; Fadel, S. M.; Sykes, E. A.; Goldaracena, N.; Kaths, J. M.; et al. Mechanism of Hard-Nanomaterial Clearance by the Liver. *Nat. Mater.* **2016**, *15*, 1212.
(4) Sørensen, K. K.; McCourt, P.; Berg, T.; Crossley, C.; Le Couteur, D. G.; Wake, K.; Smedsrød, B. The Scavenger Endothelial Cell: A New Player in Homeostasis and Immunity. *Am. J. Physiol. Regul. Integr. Comp. Physiol.* **2012**, *303*, R1217−R1230.
(5) Zhou, H.; Fan, Z.; Li, P. Y.; Deng, J.; Arhontoulis, D. C.; Li, C. Y.; Bowne, W. B.; Cheng, H. Dense and Dynamic Polyethylene Glycol Shells Cloak Nanoparticles from Uptake by Liver Endothelial Cells for Long Blood Circulation. *ACS Nano* **2018**, *12*, 10130−10141.
(6) Violatto, M. B.; Casarin, E.; Talamini, L.; Russo, L.; Baldan, S.; Tondello, C.; Messmer, M.; Hintermann, E.; Rossi, A.; Passoni, A.; et al. Dexamethasone Conjugation to Biodegradable Avidin-Nucleic-Acid-Nano-Assemblies Promotes Selective Liver Targeting and Improves Therapeutic Efficacy in an Autoimmune Hepatitis Murine Model. *ACS Nano* **2019**, *13*, 4410−4423.
(7) Yu, X.; Chen, L.; Liu, J.; Dai, B.; Xu, G.; Shen, G.; Luo, Q.; Zhang, Z. Immune Modulation of Liver Sinusoidal Endothelial Cells by Melittin Nanoparticles Suppresses Liver Metastasis. *Nat. Commun.* **2019**, *10*, 574.
(8) Marquez, J.; Fernandez-Pineiro, I.; Arauzo-Bravo, M. J.; Poschmann, G.; Stuhler, K.; Khatib, A.-M.; Sanchez, A.; Unda, F.; Ibarretxe, G.; Bernales, I.; Badiola, I. Targeting Liver Sinusoidal Endothelial Cells with miR-20a-Loaded Nanoparticles Reduces Murine Colon Cancer Metastasis to the Liver. *Int. J. Cancer* **2018**, *143*, 709−719.
(9) Cormode, D. P.; Skajaa, G. O.; Delshad, A.; Parker, N.; Jarzyna, P. A.; Calcagno, C.; Galper, M. W.; Skajaa, T.; Briley-Saebo, K. C.; Bell, H. M.; et al. A Versatile and Tunable Coating Strategy Allows Control of Nanocrystal Delivery to Cell Types in the Liver. *Bioconjugate Chem.* **2011**, *22*, 353−361.
(10) Liang, X.; Grice, J. E.; Zhu, Y.; Liu, D.; Sanchez, W. Y.; Li, Z.; Crawford, D. H.; Le Couteur, D. G.; Cogger, V. C.; Liu, X.; et al. Intravital Multiphoton Imaging of the Selective Uptake of Water-Dispersible Quantum Dots into Sinusoidal Liver Cells. *Small* **2015**, *11*, 1711−1720.
(11) Liang, X.; Wang, H.; Zhu, Y.; Zhang, R.; Cogger, V. C.; Liu, X.; Xu, Z. P.; Grice, J. E.; Roberts, M. S. Short-and Long-Term Tracking of Anionic Ultrasmall Nanoparticles in Kidney. *ACS Nano* **2016**, *10*, 387−395.
(12) Xu, G.; Zeng, S.; Zhang, B.; Swihart, M. T.; Yong, K.-T.; Prasad, P. N. New Generation Cadmium-Free Quantum Dots for Biophotonics and Nanomedicine. *Chem. Rev.* **2016**, *116*, 12234−12327.
(13) Zhang, T.; Wang, Y.; Kong, L.; Xue, Y.; Tang, M. Threshold Dose of Three Types of Quantum Dots (QDs) Induces Oxidative Stress Triggers DNA Damage and Apoptosis in Mouse Fibroblast L929 Cells. *Int. J. Environ. Res. Public Health* **2015**, *12*, 13435−13454.
(14) Scimeca, M.; Bischetti, S.; Lamsira, H. K.; Bonfiglio, R.; Bonanno, E. Energy Dispersive X-Ray (EDX) Microanalysis: A Powerful Tool in Biomedical Research and Diagnosis. *Eur. J. Histochem.* **2018**, *62*, 2841.
(15) Hunt, N. J.; Kang, S. W. S.; Lockwood, G. P.; Le Couteur, D. G.; Cogger, V. C. Hallmarks of Aging in the Liver. *Comput. Struct. Biotechnol. J.* **2019**, *17*, 1151−1161.
(16) Hunt, N. J.; McCourt, P. A.; Le Couteur, D. G.; Cogger, V. C. Novel Targets for Delaying Aging: The Importance of the Liver and Advances in Drug Delivery. *Adv. Drug Delivery Rev.* **2018**, *135*, 39−49.
(17) Hunt, N. J.; Lockwood, G. P.; Kang, S. W. S.; Pulpitel, T.; Clark, X.; Mao, H.; McCourt, P. A.; Cooney, G. J.; Wali, J. A.; Le Couteur, F. H.; Le Couteur, D. G.; Cogger, V. C. The Effects of Metformin on Age-Related Changes in the Liver Sinusoidal Endothelial Cell. *J. Gerontol., Ser. A* **2019**, *75*, 278−285, DOI: 10.1093/gerona/glz153.
(18) Hunt, N. J.; Lockwood, G. P.; Warren, A.; Mao, H.; McCourt, P. A.; Le Couteur, D. G.; Cogger, V. C. Manipulating Fenestrations in Young and Old Liver Sinusoidal Endothelial Cells. *Am. J. Physiol Gastrointest Liver Physiol* **2019**, *316*, G144−G154.
(19) Nguyen, V. H.; Lee, B.-J. Protein Corona: A New Approach for Nanomedicine Design. *Int. J. Nanomed.* **2017**, *12*, 3137.
(20) Ensign, L. M.; Cone, R.; Hanes, J. Oral Drug Delivery with Polymeric Nanoparticles: The Gastrointestinal Mucus Barriers. *Adv. Drug Delivery Rev.* **2012**, *64*, 557−570.
(21) Kim, K. S.; Suzuki, K.; Cho, H.; Youn, Y. S.; Bae, Y. H. Oral Nanoparticles Exhibit Specific High-Efficiency Intestinal Uptake and Lymphatic Transport. *ACS Nano* **2018**, *12*, 8893−8900.
(22) Wang, Y.; Zhao, Y.; Cui, Y.; Zhao, Q.; Zhang, Q.; Musetti, S.; Kinghorn, K. A.; Wang, S. Overcoming Multiple Gastrointestinal Barriers by Bilayer Modified Hollow Mesoporous Silica Nanocarriers. *Acta Biomater.* **2018**, *65*, 405−416.
(23) Kang, S. H.; Revuri, V.; Lee, S.-J.; Cho, S.; Park, I.-K.; Cho, K. J.; Bae, W. K.; Lee, Y.-k. Oral siRNA Delivery to Treat Colorectal Liver Metastases. *ACS Nano* **2017**, *11*, 10417−10429.
(24) Danielsen, E. M.; Hansen, G. H. Small Molecule Pinocytosis and Clathrin-Dependent Endocytosis at the Intestinal Brush Border: Two Separate Pathways into the Enterocyte. *Biochim. Biophys. Acta, Biomembr.* **2016**, *1858*, 233−243.
(25) Park, K.; Park, E.-J.; Chun, I. K.; Choi, K.; Lee, S. H.; Yoon, J.; Lee, B. C. Bioavailability and Toxicokinetics of Citrate-Coated Silver Nanoparticles in Rats. *Arch. Pharmacal Res.* **2011**, *34*, 153−158.
(26) Roberts, M. S.; Magnusson, B. M.; Burczynski, F. J.; Weiss, M. Enterohepatic Circulation. *Clin. Pharmacokinet.* **2002**, *41*, 751−790.
(27) Bhang, S. H.; Won, N.; Lee, T.-J.; Jin, H.; Nam, J.; Park, J.; Chung, H.; Park, H.-S.; Sung, Y.-E.; Hahn, S. K.; Kim, B.-S.; Kim, S. Hyaluronic Acid−Quantum Dot Conjugates for *In Vivo* Lymphatic Vessel Imaging. *ACS Nano* **2009**, *3*, 1389−1398.
(28) Song, R. Mechanism of Metformin: A Tale of Two Sites. *Diabetes Care* **2016**, *39*, 187−189.
(29) Nicklin, P.; Keates, A. C.; Page, T.; Bailey, C. J. Transfer of Metformin Across Monolayers of Human Intestinal Caco-2 Cells and Across Rat Intestine. *Int. J. Pharm.* **1996**, *128*, 155−162.
(30) Cogger, V. C.; Arias, I. M.; Warren, A.; McMahon, A. C.; Kiss, D. L.; Avery, V. M.; Le Couteur, D. G. The Response of Fenestrations, Actin, and Caveolin-1 to Vascular Endothelial Growth Factor in SK Hep1 Cells. *Am. J. Physiol Gastrointest Liver Physiol* **2008**, *295*, G137−G145.
(31) Tachikawa, M.; Morone, N.; Senju, Y.; Sugiura, T.; Hanawa-Suetsugu, K.; Mochizuki, A.; Suetsugu, S. Measurement of Caveolin-1 Densities in the Cell Membrane for Quantification of Caveolar

Deformation after Exposure to Hypotonic Membrane Tension. *Sci. Rep.* **2017**, *7*, 7794−7794.
(32) Rejman, J.; Oberle, V.; Zuhorn, I. S.; Hoekstra, D. Size-Dependent Internalization of Particles *via* the Pathways of Clathrin- and Caveolae-Mediated Endocytosis. *Biochem. J.* **2004**, *377*, 159−169.
(33) Ozkan Vardar, D.; Aydin, S.; Hocaoglu, I.; Yagci Acar, F. H.; Basaran, N. Effects of Silver Sulfide Quantum Dots Coated with 2-Mercaptopropionic Acid on Genotoxic and Apoptotic Pathways *In Vitro*. *Chem.-Biol. Interact.* **2018**, *291*, 212−219.
(34) Sadovnikov, S. I.; Gusev, A. I. Universal Approach to the Synthesis of Silver Sulfide in the Forms of Nanopowders, Quantum Dots, Core-Shell Nanoparticles, and Heteronanostructures. *Eur. J. Inorg. Chem.* **2016**, *2016* (31), 4944−4957.
(35) Tang, R.; Xue, J.; Xu, B.; Shen, D.; Sudlow, G. P.; Achilefu, S. Tunable Ultrasmall Visible-to-Extended Near-Infrared Emitting Silver Sulfide Quantum Dots for Integrin-Targeted Cancer Imaging. *ACS Nano* **2015**, *9*, 220−230.
(36) Mego, J. L.; McQueen, J. D. Heterolysosome Formation in Mouse Liver. *J. Cell. Physiol.* **1967**, *70*, 115−120.
(37) Hansen, B.; Longati, P.; Elvevold, K.; Nedredal, G.-I.; Schledzewski, K.; Olsen, R.; Falkowski, M.; Kzhyshkowska, J.; Carlsson, F.; Johansson, S. Stabilin-1 and Stabilin-2 are Both Directed into the Early Endocytic Pathway in Hepatic Sinusoidal Endothelium *via* Interactions with Clathrin/AP-2, Independent of Ligand Binding. *Exp. Cell Res.* **2005**, *303*, 160−173.

https://dx.doi.org/10.1021/acsnano.9b06071
ACS Nano 2020, 14, 1492−1507